Rheological properties of simple fluids by computer simulation

Denis J. Evans

Research School of Physical Science, Australian National University, P.O. Box 4, Canberra, ACT 2600, Australia and Thermophysical Properties Division, National Engineering Laboratory, National Bureau of Standards, Boulder, Colorado 80303

(Received 7 August 1980)

We present results of nonequilibrium molecular-dynamics calculations for the triple-point Lennard-Jones fluid undergoing shear flow. The calculations show that this simple fluid exhibits a wide variety of non-Newtonian behavior ranging from viscoelasticity, to shear dilatancy and flow birefringence. It is shown that the constitutive relations describing these phenomena are consistent with nonanalytic functional forms. For every property so far studied these functional forms agree with those predicted by long-time tail theories. However, the size of each effect is found to be several orders of magnitude greater than theoretical predictions.

I. INTRODUCTION

In this paper we present nonequilibrium molecular-dynamics (NEMD) results which offer a summary of the rheological properties of simple fluids. The model systems studied are: the Lennard-Jones fluid close to the triple point[1] for which which,

$$\phi = 4\epsilon\left[(\sigma/r)^{12} - (\sigma/r)^{6}\right], \tag{1}$$

and the two-dimensional soft-disk fluid close to freezing[2] for which

$$\phi = \epsilon(\sigma/r)^{12}. \tag{2}$$

The first model is known to be a reasonable approximation to the inert gas fluids. The second model fluid, while it certainly has no counterpart in nature, provides a simple means of studying the dependence of simple fluid rheological properties upon dimensionality. Recently Evans and Watts[3] have shown that the qualitative rheological properties of a wide variety of simple three-dimensional fluids are independent of the details of the interaction potential.

Most of the rheological phenomena to be discussed here can be defined in terms of the stress-strain relationship. If $\vec{P}$ denotes the pressure tensor and $\partial\vec{u}/\partial\vec{x}$ the strain rate tensor then for simple fluids in more than two dimensions and for sufficiently small strain rates the equation

$$\tilde{P}_{yx}(\omega) = \tilde{P}_{xy}(\omega) \equiv -2\tilde{\eta}(\omega)\tilde{\gamma}(\omega) \tag{3}$$

defines the complex frequency-dependent shear viscosity coefficient $\tilde{\eta}(\omega)$. In (3) "~" denotes the temporal Fourier transform and

$$\gamma \equiv (\vec{\nabla}^0\vec{u})^s_{xy} = \tfrac{1}{2}\left(\frac{\partial u_x}{\partial y} + \frac{\partial u_y}{\partial x}\right). \tag{4}$$

In three-dimensional fluids it is assumed that one can always choose a strain rate γ, sufficiently small for a *linear* isotropic coupling[4] to exist between stress and strain. It is this assumption which introduces the symmetric traceless strain rate tensor $(\vec{\nabla}^0\vec{u})^s$, which guarantees the pressure tensor is harmonic with frequency ω (no sub or super harmonics) and which also implies that Eq. (3) is complete. The other elements of the pressure tensor take on their equilibrium values. The zero-frequency Newtonian stress-strain relationship follows immediately from (3).

$$P_{xy} = P_{yx} = -2\tilde{\eta}(0)\gamma. \tag{5}$$

It is assumed that for sufficiently small γ, $\tilde{\eta}(0)$ is a function only of thermodynamic variables. Equations (3) and (5) therefore describe *linear* relationships between the pressure tensor and the strain rate tensor.

In the nonlinear regime (large γ for three-dimentional systems) if the strain rate tensor is given as

$$\partial\vec{u}/\partial\vec{x} = \begin{pmatrix} 0 & 2\gamma & 0 \\ 0 & 0 & 0 \\ 0 & 0 & 0 \end{pmatrix}, \tag{6}$$

then at zero frequency the pressure tensor can be written as,[5]

$$P = \begin{pmatrix} p_{zz}(\gamma) + \sigma_1(\gamma), \eta(\gamma)\gamma & 0 \\ \eta(\gamma)\gamma, & p_{zz}(\gamma) + \sigma_2(\gamma) & 0 \\ 0 & 0 & p_{zz}(\gamma) \end{pmatrix}. \tag{7}$$

In this complicated constitutive relation $\eta(\gamma)$ is the zero-frequency nonlinear, effective shear viscosity coefficient. The hydrostatic pressure $p(\gamma)$ is given as

$$p(\gamma) = \tfrac{1}{3}\,\mathrm{tr}(P) = P_{zz} + \tfrac{1}{3}(\sigma_1 + \sigma_2).$$

In the nonlinear regime the hydrostatic pressure is a function not only of the usual thermodynamic variables (temperature and density, T and ρ) but

of the strain rate as well.[6] This effect is known as shear dilatancy and is usually observed experimentally as a change in density with strain rate under constant pressure and temperature.[7] The σ_i variables describe the differences in the normal stresses that occur under high rates of shear. These normal stress effects are believed responsible for non-Newtonian phenomena such as the Weissenberg effect.[5,7] In the linear regime the eigenvectors of the pressure tensor are at 45° to the x, y axes. It is easily seen that in the nonlinear regime the directions of maximum and minimum stress make angles Θ_i to the x axis where

$$\tan\Theta_i = \frac{-(\sigma_1-\sigma_2)\pm[(\sigma_1-\sigma_2)^2+4\eta^2\gamma^2]^{1/2}}{2\eta\gamma} . \quad (8)$$

A group of related theories[8] which we shall call "long-time tail theories," attempt to predict the leading terms of non-Newtonian behavior from a knowledge of the equilibrium and Newtonian properties of the system. The mechanism by which these properties are believed to determine the leading non-Newtonian behavior (both linear and nonlinear) involves slowly decaying hydrodynamic processes—the so-called long-time tails that were first discovered by Alder, Gass, and Wainwright.[9] These asymptotic predictions (asymptotic in ω and γ) are summarized in Table I. One of the most significant implications of these predictions is that the pressure tensor is a nonanalytic function of both frequency and strain rate. In two dimensions these nonanalytic cusps are predicted to become stronger and the Newtonian shear viscosity is thought to diverge logarithmically as both a function of frequency and strain rate.[8]

By performing computer simulations of shear flow (nonequilibrium molecular dynamics) we have recently found support for the functional forms predicted theoretically for both two- and three-dimensional systems. We produced the first computer simulation evidence for a square-root cusp in the frequency-dependent shear viscosity.[10] Later more accurate calculations for the Lennard-Jones fluid at moderate densities shows that over two octaves in frequency the square-root dependence fitted the observed results with a maximum relative error of ~4 percent.[11]

TABLE I. Asymptotic non-Newtonian behavior of three-dimensional systems. $\eta(0)\equiv\tilde{\eta}(0)$. Long-time tail theories give expressions for the various A constants in terms of thermodynamic and Newtonian transport properties. "i" in (b1) is $\sqrt{-1}$.

a. Limiting (small γ) nonlinear behavior

$$p(\gamma)=p(0)+A_p|\gamma|^{3/2}, \quad (a1)$$

$$\sigma_i(\gamma)=A_{\sigma_i}|\gamma|^{3/2}, \quad (a2)$$

$$\eta(\gamma)=\eta(0)-A_\eta|\gamma|^{1/2}, \quad (a3)$$

b. Limiting (small ω) linear viscoelastic behavior

$$\tilde{\eta}(\omega)=\tilde{\eta}(0)-(1+i)A_{\tilde{\eta}}\omega^{1/2} \quad (b1)$$

Our earlier frequency-dependent studies were limited to moderate densities away from the freezing line, because as Ashurst and Hoover[12] have shown complicating nonlinear effects are magnified at high densities. In this paper we present the results of accurate Lennard-Jones triple-point calculations both as a function of frequency (after extrapolation to zero strain rate) and as a function of strain rate (at zero frequency). A preliminary account of the zero-frequency results showing that over almost two decades in strain rate Eq. (a3) in Table I fits the nonlinear results to better than 3 percent has been published earlier.[13]

In spite of the fact that so far the results indicate agreement between the predicted (Table I) and observed *functional forms* there has been a discrepancy of more than 2 orders of magnitude regarding the values of the coefficients, A_i (Table I). The computer results may be calculated at strain rates and frequencies too high for the asymptotic theories to be appropriate. However, we have recently calculated the nonlinear viscosity and hydrostatic pressure for a two-dimensional system.[14] For both properties we observed the predicted logarithmic dependences but again the coefficients of the predicted and observed functional forms disagree by several orders of magnitude.

The "coincidences" between the observed and predicted asymptotic functional forms and the disagreements regarding the magnitudes of these effects are not limited to the results of nonequilibrium molecular-dynamics simulations of shear flow. Recently Wood and Erpenbeck[15] have used equilibrium molecular dynamics to calculate the limiting ($\omega\to 0$) form for $\tilde{\eta}(\omega)$ using the Kubo-Green expression.[8] They find a square-root cusp some 400 times larger than theoretical predictions. Hoover, *et al.*[16] have simulated cyclic compression in the triple-point Lennard-Jones fluid to calculate the limiting frequency dependence of bulk viscosity. Again the data are consistent with a square-root cusp several orders of magnitude greater than expected.

In this paper we complement and extend our previous work. We show that at the triple point the Lennard-Jones fluid exhibits a large square-root cusp for $\tilde{\eta}(\omega)$. We detail more accurate and complete results for the square-root strain rate dependence of $\eta(\gamma)$ than has been published before; we show that the shear dilation effect varies as

$\gamma^{3/2}$ (a1); we provide data for normal stress differences σ_i and finally we provide data for the nonequilibrium radial distribution functions both of two- and three-dimensional systems.

II. METHOD

Detailed descriptions of the simulation algorithm have been published previously.[10,11,13] Consequently we give only the briefest description here. The equations of motion of N particles interacting through either the Lennard-Jones (1) or the soft-disk (2) potential, are solved subject to oblique periodic boundary conditions which constrain the system to planar Couette flow. A thermostat removes the viscous heat produced at each timestep ensuring that the system is isothermal. The constitutive relations[3,5,7] are used together with the statistical mechanical expressions for the pressure and strain rate tensors to calculate the required transport coefficients. At low strain rates where the signal-to-noise ratio deteriorates the first moment of the peculiar velocity is adjusted (in addition to the second moment which gives the temperature) to set the required strain rate.

The simulation parameters for the Lennard-Jones (1) and soft-disk (2) work described in this paper are set out in Table II.

III. NONLINEAR EFFECTS IN THE LENNARD-JONES FLUID

A. Shear thinning behavior

Figure 1 shows the computed zero-frequency effective viscosity as a function of the *square root* of the strain rate. The data are consistent with a square-root dependence

$$\eta(\gamma) = 3.17\,(\pm 0.03) - 1.48(\pm 0.05)|\,\gamma|^{1/2}\,. \qquad (9)$$

Over a 100-fold range in strain rate the maximum relative error is 2.5 percent and the correlation coefficient is 0.989. The data for Fig. 1 are given in Table III. As can be seen in the table the number of timesteps used for each run varied approximately linearly with γ^{-1}. The calculation at the lowest strain rate was carried out to 520 000 timesteps and is one of the longest real time simulations that has been performed for a continuous potential.

TABLE II. Simulated parameters.

	Lennard-Jones	Soft disk
System size: N	108	32
$\phi(r)$ truncation: r_c^*	2.5	1.5
time step: Δt^*	0.007	0.007
density: ρ^*	0.8442	0.9238
temperature: T^*	0.722	1.0
Units: System properties are calculated in dimensionless units. Values are reduced by ϵ, σ, m = particle mass		
density: $\rho^* =$	$\rho\sigma^3$	$\rho\sigma^2$
temperature: $T^* =$	kT/ϵ	kT/ϵ
time: $t^* =$	$t(\epsilon/m)^{1/2}\sigma^{-1}$	$t(\epsilon/m)^{1/2}\sigma^{-1}$

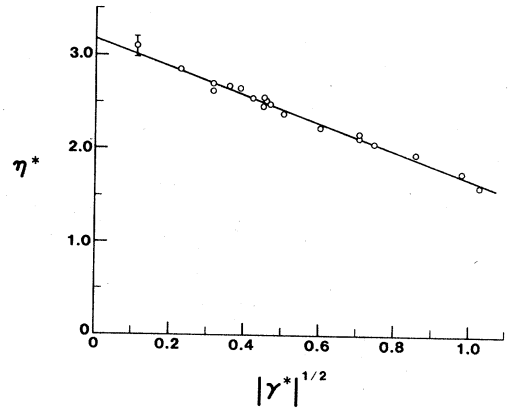

FIG. 1. Shear viscosity η^* is plotted as a function of the square root of the strain rate $|\gamma^*|^{1/2}$.

Three data points were obtained for a 256-particle system. As can be seen from Table III the results for $N = 256$ agree with those for $N = 108$ within estimated statistical uncertainties. These size dependence checks confirm results by Hoover and Ashurst[17] and Hoover, *et al.*[16] showing a negligible size dependence for this system using the homogeneous shear algorithm.

B. Normal stress effects

Table III also shows the strain rate dependence of the hydrostatic pressure p and the normal stress differences σ_1, σ_2. Figure 2 gives a log-log plot of $p(\gamma)$ against the strain rate. As can be seen the data are consistent with the predicted asymptotic form. When fitted to the $\gamma^{*3/2}$ functional form we find that

$$p(\gamma^*) = 1.018 + 2.601|\,\gamma|^{3/2}\,. \qquad (10)$$

The correlation coefficient for the fit ($\gamma^* < 0.6$) is 0.997. We note that this equation was obtained for a Lennard-Jones potential truncated at $r = 2.5\sigma$.

The data for the normal stress differences are much poorer in quality. Figure 3 shows a graph of σ_1, σ_2 as a function of $\gamma^{3/2}$. If we assume this relationship is linear (a2) we find that

$$\sigma_1(\gamma^*) = 0.008 + 1.13|\,\gamma|^{3/2}\,, \qquad (11)$$

and

TABLE III. Nonlinear shear flow properties of the triple-point Lennard Jones fluid. (1) $N = 108$ (2) $N = 256$.

$\gamma\sigma(m/\epsilon)^{1/2}$	$\eta\sigma^2/(m\epsilon)^{1/2}$	$\rho(\sigma^3/\epsilon)$	$\sigma_1(\sigma^3/\epsilon)$	$\sigma_2(\sigma^3/\epsilon)$	Timesteps	Notes
					(10^{-3})	
0.0513	2.844	1.025	0.021	0.066	37	1
0.1006	2.605				20	1
0.1491	2.656				20	1
0.1745	2.542				15	1
0.2505	2.383				10	1
0.4952	2.135				8	1
0.9569	1.744				8	1
0.1995	2.552	1.384				2
0.2041	2.458	1.259				2
0.4905	2.163	2.007				2
0.0		0.997			20	1
0.0126	3.099				524	1
0.0980	2.692	1.074	0.04	0.07	23	1
0.1992	2.551	1.298	0.13	0.24	20	1
0.2031	2.468	1.283	0.12	0.10	25	1
0.3606	2.213	1.608	0.18	0.32	27	1
0.5565	2.062	2.085	0.50	0.56	12	1
0.7313	1.954				8	1
1.051	1.596	3.11	0.79	0.91	14	1

$$\sigma_2(\gamma^*) = 0.033 + 1.29\,|\,\gamma\,|^{3/2}\,. \tag{12}$$

The constant term in (11) and (12) must of course be zero (since fluids must have an isotropic pressure tensor at equilibrium). Within statistical uncertainties this consistency requirement is satisfied. In view of the statistical uncertainties, the difference between the sizes of the $\gamma^{3/2}$ terms is hardly significant. If we assume that at $\gamma^* = 1$, the data still follow the functional forms in Table I then Eq. (8) implies that the eigenvectors of the pressure tensor have rotated through only 1.4°.

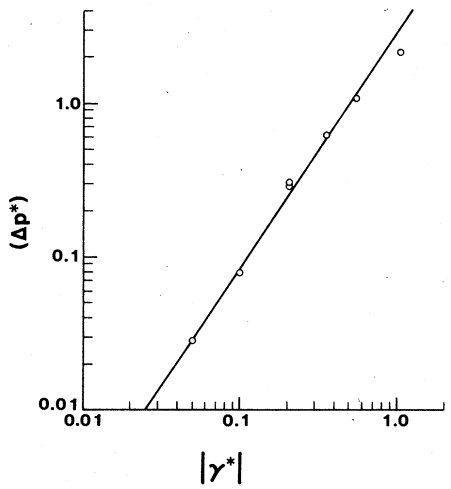

FIG. 2. We show a $\log_{10}$-$\log_{10}$ plot of the shear induced pressure change as a function of strain rate. The straight line is Eq. (10).

IV. VISCOELASTICITY AT THE LENNARD-JONES TRIPLE POINT

As pointed out earlier[10] one can simulate sinusoidal time-dependent shear flow to calculate the frequency-dependent shear viscosity. This is a reasonable procedure only if one carries it out for as small an amplitude as possible since at large amplitudes where nonlinear effects are present one knows that if the strain rate is harmonic with frequency ω then the pressure tensor will contain super harmonics at 2ω, 4ω, etc. The amplitudes studied in this work were sufficiently small for the harmonic distortion to be $\lesssim 1\%$.

Table IV shows details of the calculation of

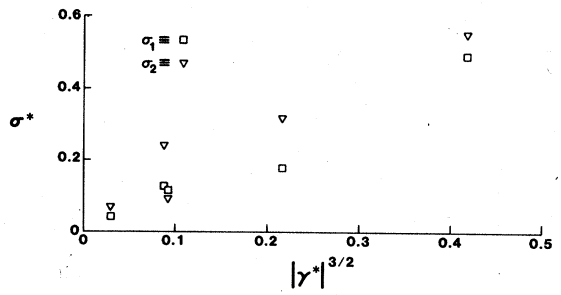

FIG. 3. The normal stress differences are plotted against the strain rate to the $\frac{3}{2}$ power. Note: $\sigma_1 = P_{xx} - P_{zz}$, $\sigma_2 = P_{yy} - P_{zz}$.

TABLE IV. $\tilde{\eta}(\omega)$ at the LJ triple point. Above $\omega^*=17$ we use $\Delta^*=0.002$ rather than 0.007.

γ^*	$\tilde{\eta}_r^*$	$\tilde{\eta}_I^*$	ω^*	$t(10^{-3}S)$	Δt^*
0.1	2.704	0.70	1.122	40	0.007
0.1	2.212	0.70	2.24	20	0.007
0.1	2.14	0.91	2.24	20	0.007
0.1	1.736	1.07	4.49	20	0.007
0.1	1.223	1.00	8.976	20	0.007
0.1	1.145	0.97	11.97	20	0.007
0.1	1.054	0.98	11.97	20	0.007
0.1	0.900	0.92	14.96	20	0.007
0.15	2.409	0.60	1.122	26	0.007
0.15	2.334	0.76	2.244	32	0.007
0.15	1.719	0.97	4.489	20	0.007
0.15	1.253	0.94	8.976	20	0.007
0.15	1.137	0.94	11.968	20	0.007
0.0502	2.548 ±0.04	0.614	1.22	503	0.007
0.0510	2.189	1.024	2.244	84	0.007
0.049	1.269	0.98	8.98	77	0.007
0.0501	1.013	0.83	11.968	77	0.007
0.1	0.346	0.721	31.42	20	0.002
0.1	0.506	0.883	22.44		0.002
0.1	0.663	0.949	19.64	10	0.002
0.1	0.411	0.795	26.18	14	0.002
0.1	0.237	0.624	39.27	16	0.002
0.1	0.829	0.941	17.95	20	0.002

$\tilde{\eta}(\omega)$. The real and imaginary parts of $\tilde{\eta}$ were calculated by noting the phase and amplitude relations of stress and strain. The calculations were performed for three different amplitudes and as can be seen from Table IV there is no systematic amplitude dependence of $\tilde{\eta}(\omega)$. It appears that the amplitude dependence of $\tilde{\eta}(\omega,\gamma)$ has essentially vanished for $\omega^* \gtrsim 1$ and $\gamma^* \leq 0.15$.

Two different timesteps were used for the solution of the equation of motion. This is required since for $\omega^* \gtrsim 17$ the motion of the periodic images is so rapid that a significant displacement can occur in a single timestep ($\Delta t^* = 0.007$). It was found by trial and error that reducing the timestep to $\Delta t^* = 0.002$ above $\omega^* = 17$ produced consistent sets of results that smoothly mesh into one another.

As is well known the real and the imaginary parts of $\tilde{\eta}(\omega)$ are not independent but are related by the Kramers-Kronig relationship

$$\mathrm{Re}[\tilde{\eta}(\omega)] = \frac{-2}{\pi}\int_0^\infty \frac{\omega' \,\mathrm{Im}[\tilde{\eta}(\omega')]}{\omega'^2-\omega^2}\,d\omega', \qquad (13)$$

$$\mathrm{Im}[\tilde{\eta}(\omega)] = \frac{-2}{\pi}\int_0^\infty \frac{\omega\,\mathrm{Re}[\tilde{\eta}(\omega')]}{\omega^2-\omega'^2}\,d\omega' . \qquad (14)$$

By looking at the data in Table IV we see that the statistical fluctuations (particularly for small ω) in the imaginary component are approximately twice those of the real. Thus most of the subsequent discussion concerns $\tilde{\eta}_R(\omega) \equiv \mathrm{Re}\,\tilde{\eta}(\omega)$.

Figure 4 shows a graph of $\tilde{\eta}_R(\omega)$ as a function of the *square root* of the frequency. As can be seen at low frequencies the data are linear in $\omega^{*1/2}$. A reassuring result is that if one fits the lowest nonzero-frequency data to Eq. (b1) one finds that the extrapolated $\tilde{\eta}(0)$ agrees almost exactly with the value obtained by extrapolating the zero-frequency results to zero-strain rate, (namely 3.15 and 3.17, respectively).

Although for $\omega^* > 1$ there appears to be no amplitude dependence because

$$\lim_{\omega\to 0} \tilde{\eta}_R(\omega,\gamma) = \eta(\gamma) = \eta(0) - A_\eta |\gamma|^{1/2} . \qquad (15)$$

In Fig. 4 we have sketched in the limiting zero-frequency values $\eta(\gamma)$ for the three values of γ used in this work. The data have been interpolated using the equation

$$\mathrm{Re}[\tilde{\eta}^*(\omega^*,\gamma^*)] = 3.15 - (0.178\,\omega^{*2} + 4.798\,\gamma^{*2})^{1/4} . \qquad (16)$$

In looking for the most compact means of summarizing the data in Table IV we noted immediately that the data in Fig. 4 can be successfully fit to a power series expansion in odd half-integer powers of ω,

$$\tilde{\eta}_R(\omega) = \tilde{\eta}(0) + \tilde{\eta}_1\omega^{1/2} + \tilde{\eta}_3\omega^{3/2} + \tilde{\eta}_5\omega^{5/2} + \cdots . \qquad (17)$$

Now either by using the calculus of residues and the Kramers-Kronig relationshps or by insisting that the Laplace transform $\eta(s) = \tilde{\eta}(\omega = s/i)$ is real, one can deduce an asymptotic expansion for $\tilde{\eta}_1$,

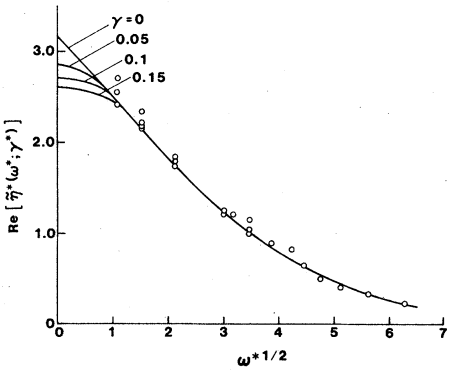

FIG. 4. The real part of the shear viscosity is plotted against the square root of the frequency. For nonzero frequencies there is no systematic strain rate dependence. The curves are given by Eq. (16) for the strain rates indicated.

$$\tilde{\eta}_I(\omega)=\tilde{\eta}_1\omega^{1/2}-\tilde{\eta}_3\omega^{3/2}+\tilde{\eta}_5\omega^{5/2}+\cdots . \quad (18)$$

Inverting (17) and (18) we obtain the stress-stress time-correlation function $\eta(t)$. Using the Tauberian theorems[18] one has

$$\lim_{t\to\infty}\eta(t)=\frac{1}{2\sqrt{\pi}}\{-\tilde{\eta}_1 t^{-3/2}-\tfrac{3}{2}\tilde{\eta}_3 t^{-5/2}+\tfrac{15}{4}\tilde{\eta}_5 t^{-7/2}+\cdots\}. \quad (19)$$

It is important to note that it is only the half integer components of the power series for $\tilde{\eta}(\omega)$ which contribute to the asymptotic long-time behavior of $\eta(t)$. These are the only terms needed to fit our data.

A more usual approach to fitting such spectra is through the moment expansion[19]

$$\frac{d^n\eta}{dt^n}(t=0)=\frac{1}{2\pi}\int_{-\infty}^{+\infty}\frac{(i\omega)^n}{n}\tilde{\eta}(\omega)d\omega . \quad (20)$$

It is easily seen, however, that this theorem is useless for fitting our results since even for the second moment at least 50% of the integral (20) is determined by frequencies higher than the highest studied in this work ($\omega^*=40$). This is a consequence of the small radius of convergence of the Taylor expansion of $\eta(t)$.

Although the half-integer expansion of $\tilde{\eta}(\omega)$[17,18,19] works quite well we found a more compact way to summarize the data. If we assume, using (19) as a guide,

$$\eta(t)=\frac{G_\infty}{e^{-t/\tau}+(G_\infty t^{3/2}/A\tilde{\eta})}, \quad (21)$$

we see that we can guarantee: The correct value for $\eta(t=0)$ which must be the infinite frequency shear modulus G_∞; the correct coefficient of the $\omega^{1/2}$ cusp of $\tilde{\eta}(\omega)$ [*NB*: $A\tilde{\eta}=-\tilde{\eta}_1$ in Eq. (17)] and we can choose τ to obtain the correct value for the zero-frequency shear viscosity. The smooth curve drawn through the data points in Fig. 4 shows the spectrum obtained with $G_\infty^*=24.89$ (the known value for the modulus[20]), $A\tilde{\eta}^*=0.65$ (the measured asymptotic slope of the data in Fig. 4) and $\tau^*=0.12$. This choice for the time-correlation function fits all of our data for both $\tilde{\eta}_R(\omega)$ and $\tilde{\eta}_I(\omega)$ within estimated uncertainties. It predicts $\tilde{\eta}(0)=3.15$. Figure 5 shows a graph of both the real and imaginary parts of $\tilde{\eta}$ so obtained. It is interesting to note that the region over which the asymptotic square-root behavior occurs is relatively larger for $\tilde{\eta}_R$ than for $\tilde{\eta}_I$.

In Fig. 6 we show the time-correlation function $\eta(t)$. Because our function for $\eta(t)$ only involves three adjustable constants and was fitted from a necessarily noisy spectrum it should not be regarded as a basic output of our simulation.

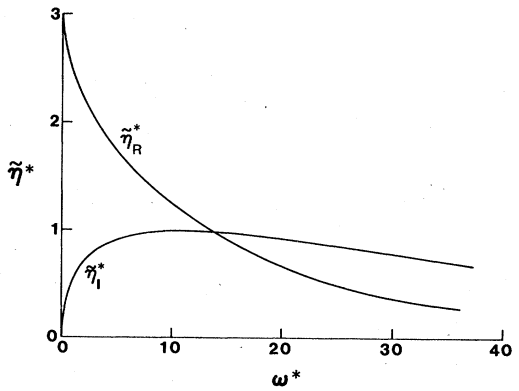

FIG. 5. Shows the complex viscosity [Eq. (21)] as a function of frequency. This equation is consistent with all the extrapolated zero strain rate data.

The time-correlation function can be regarded as the impulse response function since

$$P_{xy}(t)=-2\int_0^\infty \eta(t-\tau)\gamma(\tau)d\tau , \quad (22)$$

$\eta(t)$ predicts the response of the system to an impulse in the strain rate. We also show $N(t)$, the step response function, $N(t)=\int_0^t \eta(t')\,dt'$. It is important to realize how slowly the Kubo-Green integrand converges. After 150 timesteps (or $t^*=1.0$) $N(t)$ is 13% below its asymptotic value. After 1500 timesteps (or $t^*=10.0$) it is still 5% below its asymptotic value. Many early computer simulations of equilbrium properties were less than 2,000 timesteps long.

V. SHEAR BIREFRINGENCE

For simple fluids undergoing shear flow the singlet-distribution function maintains its equilibrium value. This is not true for the two-particle

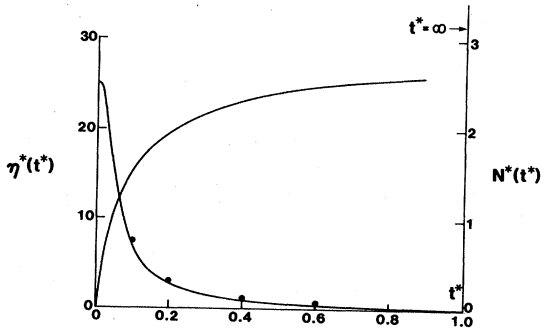

FIG. 6. Shows the stress time-correlation function $\eta(t)$ and the step response function $N(t)$ generated using Eq. (21). The crosses denote Levesque's (Ref. 26) equilibrium computer simulation results at intermediate times. Note the slow decay of these functions.

distribution function, $g(\vec{r},\gamma)$. Assuming $g(\vec{r};\gamma)$ is suitably smooth in angles $(\hat{r})$ but not necessarily in strain rate γ, we may expand in spherical harmonics.[20]

$$g(\vec{r};\gamma)=\sum_{m,n} A_{m,n}(r;\gamma)Y^{e}_{m,n}(\theta,\phi)+B_{m,n}(r;\gamma)Y^{0}_{m,n}(\Theta,\phi)\,, \tag{23}$$

where

$$Y^{0}_{m,n}=\cos(m\phi)P^{m}_{n}(\cos\Theta)\,,$$

and

$$Y^{0}_{m,n}=\sin(m\phi)P^{m}_{n}(\cos\Theta)\,,$$

are the even-and odd-spherical harmonics. Our notation is that of Morse and Feshbach.[20] Integrals over $g(\vec{r};\gamma)$ can be expressed as ensemble averages since

$$\int d\vec{r}\,' f(\vec{r}\,')\delta(|\vec{r}-\vec{r}\,'|)\rho g(\vec{r}\,';\gamma)=4\Pi\langle r^2 f(\hat{r})\rangle_{r,r+dr}\,. \tag{24}$$

The angle brackets denote the nonequilbrium ensemble average in a spherical shell of radius $r, r+dr$. Using the orthogonality properties of spherical harmonics we can write expressions for the expansion coefficients as ensemble averages.

$$A_{m,n}(r\gamma)=\frac{\epsilon_m(2n+1)(n-m)!}{4\pi\rho(n+m)!r^2}\langle Y^{e}_{m,n}\rangle_{r,r+dr}\,, \tag{25}$$

$$B_{m,n}(r\gamma)=\frac{\epsilon_m(2n+1)(n-m)!}{4\pi\rho(n+m)!r^2}\langle Y^{o}_{m,n}\rangle_{r,r+dr}, \tag{26}$$

where $\epsilon_m=1$ if $m=0$, $=2$ otherwise. From the parity of $g(\vec{r};\gamma)$ if n is odd, $A_{m,n}$, $B_{m,n}$ vanish for all r,γ. This expansion (23) exists provided the angular variation of $g(\vec{r};\gamma)$ is sufficiently smooth.[20] It does not require smoothness with respect to γ or r.

In previous work we have used the irreducible Taylor expansion of $g(\vec{r};\overset{0}{\gamma}{}^{s})$ as introduced by Green.[21] It predicts,

$$g(\vec{r};\overset{0}{\gamma}{}^{s})=g(r;\gamma=0)+\left(\frac{\partial g}{\partial\overset{0}{\gamma}{}^{s}}\right)_{\overset{0}{\gamma}{}^{s}=0}:\overset{0}{\gamma}{}^{s}+O(\gamma^2) \tag{27}$$

$$=g(r)+\nu(r)T^{2}\left(\frac{\vec{r}}{r}\right):\overset{0}{\gamma}{}^{s}+O(\gamma^2)\,, \tag{28}$$

where $T^{(2)}$ is the symmetric traceless second-rank tensor

$$T^{(2)}=\frac{\vec{r}\vec{r}-\frac{1}{3}r^2\underline{I}}{r^2}\,. \tag{29}$$

For this expansion to exist $g(\vec{r};\overset{0}{\gamma}{}^{s})$ must be analytic in the strain rate at $\overset{0}{\gamma}{}^{s}=0$. This is probably not so since the pressure and the shear viscosity, which are integrals of $g(\vec{r};\gamma)$, are presumably nonanalytic in γ. The divergence of the Green expansion was first realized by Evans and Watts.[3]

Nevertheless by allowing the coefficients of (27) to be functions of γ we can obtain useful information regarding the γ-dependent structure for fluids undergoing shear.[3,22] In fact one can identify the $g(r;\gamma)$ and $\nu(r;\gamma)$ terms in the spherical harmonic expansion.

$$g(r;\gamma)=A_{00}(r;\gamma)\,, \tag{30}$$

$$\nu(r;\gamma)=3B_{22}(r;\gamma)/\gamma\,. \tag{31}$$

By integrating the spherical harmonic expansion one can see that the hydrostatic pressure p is given by the equation

$$p=\rho kT+\frac{2\pi}{3}\rho^2\int_0^\infty r^3\phi'(r)A_{00}(r,\gamma)dr\,. \tag{32}$$

The potential contribution to the shear viscosity η^{ϕ} is given as

$$\eta=\frac{2\pi\rho^2}{5}\int_0^\infty r^3\phi'(r)\frac{B_{22}(r;\gamma)}{\gamma}dr\,. \tag{33}$$

The normal stress differences are given by the equations

$$\sigma_1=-\frac{\pi\rho^2}{5}\int_0^\infty dr\,r^3\phi'(r)[4A_{22}(r;\gamma)-A_{02}(r;\gamma)]\,, \tag{34}$$

and

$$\sigma_2=\frac{\pi\rho^2}{5}\int_0^\infty dr\,r^3\phi'(r)[4A_{22}(r;\gamma)+A_{02}(r;\gamma)]\,. \tag{35}$$

The introduction of spherical harmonics allows a simple qualitative description of the parts of $g(\vec{r};\gamma)$ which give rise to the various macroscopic effects.[30]

As we showed in Sec. IV the normal stress differences as calculated in our computer simulations are subject to relatively large statistical fluctuations. Consequently we will not give details of their corresponding expansion coefficients, A_{22} and $A_{02}(r;\gamma)$.

In view of the asymptotic relations for $p(\gamma)$ and $\eta(\gamma)$ given in Table I, we might expect that

$$A_{00}(r;\gamma)=g(r;\gamma)=g_0(r)+g_1(r)\,|\gamma|^{3/2}\,, \tag{36}$$

and

$$\frac{3B_{22}(r;\gamma)}{\gamma}=\nu(r;\gamma)=\nu_0(r)+\nu_1(r)\,|\gamma|^{1/2}\,. \tag{37}$$

This conjecture turns out to be consistent with the simulation results. Figures 7 and 8 show $g_0(r)$, $g_1(r)$, and $\nu_0(r)$, $\nu_1(r)$ as a function of separation.

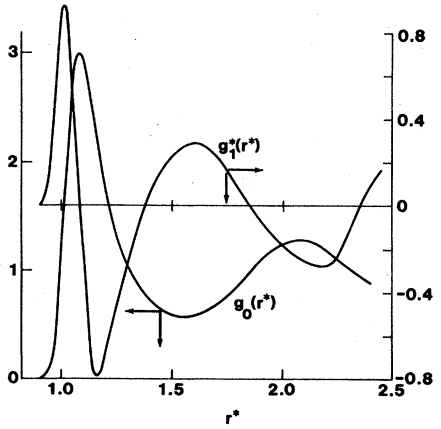

FIG. 7. $g_0(r^*)$ and $g_1(r^*)$ are plotted as a function of reduced separation r for the triple-point Lennard-Jones system. Note that the equilibrium radial distribution function $g_0(r^*)$ was obtained without using any equilibrium data.

$g_0(r)$ is of course the equilibrium radial distribution function for the triple-point Lennard-Jones fluid. However the $g_0(r)$ displayed in Fig. 7 was *not* obtained from any equilibrium data. Thus the agreement of the graphed $g_0(r)$ with the well known $g(r)$ for this state point [23] constitutes a good check on the validity of (36). As has been pointed out by Evans and Watts (Ref. 3), $\nu_0(r)$ is given approximately by $-[G_\infty/\tilde{\eta}(0)]r dg_0/dr$.

By way of contrast we also show graphs of $g(r;\gamma)$ and $\nu(r;\gamma)$ for the soft-disk fluid. As has been reported by Evans[14] computer simulations are consistent with a logarithmic divergence of shear viscosity in two dimensions,

$$\eta(\gamma) = A_\eta \log|\gamma\tau_\eta| \tag{38}$$

and a logarithmic pressure dependence

$$p(\gamma) = p(0) + Ap\,|\gamma\tau_p|\log|\gamma\tau_p|\,. \tag{39}$$

Thus by analogy with three-dimensional fluids we might expect that in two dimensions

$$\nu(r;\gamma) = A_\nu(r)\log|\gamma\tau_\nu(r)|\,,$$

and

$$g(r\gamma) = g_0(r) + A_g(r)\,|\gamma\tau_g(r)|\log|\gamma\tau_g(r)|\,. \tag{40}$$

In fact the nonequilibrium radial distribution function is consistent with a simpler form than (41). The data are consistent with the equation

$$g(r;\gamma) = g_0(r) + A_g(r)\,|\gamma\tau_p|\log|\gamma\tau_p|\,. \tag{41}$$

Figures 9 and 10 show

$$A_g(r)\tau_p \equiv g_1(r), A_\nu(r)\log\tau_\nu(r) \equiv \nu_0(r)\,,$$

and

$$A_\nu(r) \equiv \nu_1(r)\,, \tag{42}$$

for a periodic system of 50 soft spheres. Note that for this system $\tau_p^* = 11.09$.[14] Equation (42) has some important consequences for the nonlinear irreversible thermodynamics of two-dimensional fluids. If (42) is correct then *all* configurational thermodynamic properties that depend solely on the zeroth-order spherical harmonic Y_{00}^e (like internal energy and pressure) take on their equilibrium values at the same nonzero strain rate $\gamma = 1/\tau_p$. Since in the constant temperature ensemble the kinetic contributions to internal energy and pressure are independent of strain rate, we find that at $\gamma = 1/\tau_p$ the internal energy and the

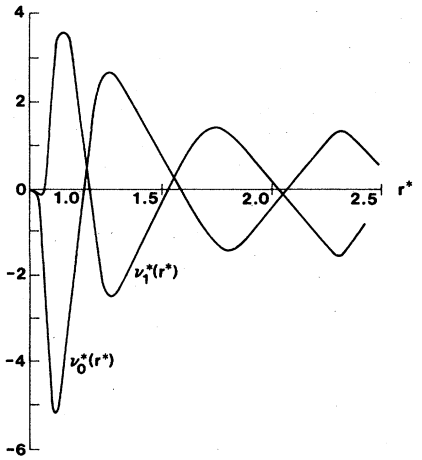

FIG. 8. Shows that part of the Lennard-Jones radial distribution function which determines the potential contribution to the linear and nonlinear shear viscosity coefficients (ν_0, ν_1).

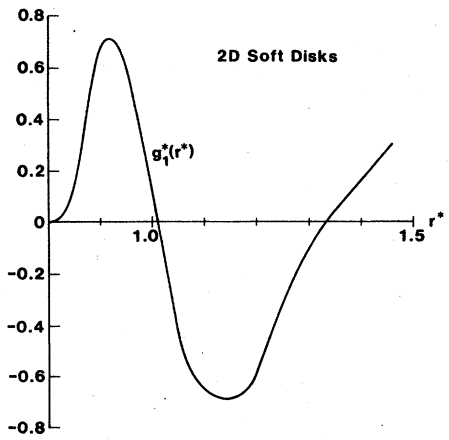

FIG. 9. $g_1(r^*)$ is the nonlinear spherical contribution to the soft-disk radial distribution function. $g_1(r) = A_g(r)\tau_p$ where $\tau_p^* = 11.09$[4] (see text). Note that $\tau_g(r) = \tau_p$ independent of r within numerical uncertainties.

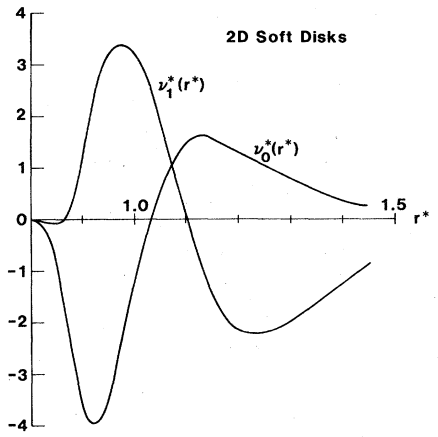

FIG. 10. ν_0 and ν_1 are the two components of the anisotropic nonequilibrium radial distribution function responsible for the soft-disks shear viscosity. $\nu_0(r) = A_\nu(r)\log_{10}\tau_\nu(r)$, $\nu_1(r) \equiv A\,\nu(r)$ (see text).

hydrostatic pressure both take on the equilibrium values.

VI. CONCLUSION

The results described in this paper show that all fluids can be expected to be non-Newtonian. Fluids such as argon are observed to be Newtonian only because macroscopic turbulence prevents the attainment of sufficiently high strain rates for the kinds of nonlinear effects described in this paper to be observed. Computer simulation overcomes this difficulty by providing a microscopic system where macroscopically large strain rates can be used to study nonlinear laminar flow in simple fluids.

Although the nonlinear effects described here are at present experimentally inaccessible they may nonetheless provide vitally important information for the theoretical understanding of both the non-Newtonian behavior of complex fluids and the Newtonian behavior of simple fluids. The observed, apparently nonanalytic, constitutive relations and their connection with linear "long-time tail" phenomena underscore this point.

It might be objected that our simulations, which are run isothermally, do not present the "true" nonlinear behavior of real fluids (provided turbulence could be supressed by for example constructing viscometers with a very small characteristic lengths) since these calculations ignore the effects of viscous heating. However since the heating is for small γ, proportional to γ^2 and *every* nonlinear effect discussed in our work is of lower order in γ (e.g., $\gamma^{3/2}$, $\gamma\log\gamma$), we believe that the qualitative features of the nonlinear phenomena discussed here should be independent of whether the experiments are performed isothermally or adiabatically.

We note that nonequilibrium radial distribution functions are likely to be of considerable future importance since they have recently been measured by Clark and Ackerson[24] and they have been related to equilibrium time-correlation expressions by Evans, *et al.*[25]

Finally we would like to mention that a direct outcome of the simulation of nonlinear Couette flow has been the development of nonlinear thermodynamics.[6] In this theory the strain rate γ is incorporated as an additional thermodynamic state variable. It provides a general framework within which the connections between shear dilatancy as observed in different ensembles and shear induced internal energy changes are explained. It provides an understanding of shear-induced phase changes[27] which have recently been observed experimentally.[28] It has also lead to a proof of the nonanalytic nature of the shear dilatancy constitutive relation.[29]

ACKNOWLEDGMENT

The author wishes to thank the Computer Centre, the R.S. Phys. S. Computer Unit and the Joint Schools computer centre at the Australian National University for large allocations of computer time on the three machines which performed the simulations described in this paper. The author also acknowledges the partial support of a Fellowship from the Fulbright Foundation.

[1]J. P. Hansen and L. Verlet, Phys. Rev. 184, 151 (1969).
[2]W. G. Hoover, W. T. Ashurst, and R. J. Olness, J. Chem. Phys. 60, 4043 (1974).
[3]D. J. Evans and R. O. Watts, Chem. Phys. 48, 321 (1980).
[4]Linear isotropic coupling of thermodynamic forces and fluxes is giverned by "Curies' Principle," see S. R. de Groot and P. Mazur, *Nonequilibrium Thermodynamics* (North-Holland, Amsterdam, 1962).
[5]H. Markovitz, *Nonlinear Steady-Flow Behavior,* Chap. 6 in *Rheology* 4, edited by F. R. Eirich (Academic, New York, 1967).
[6]The consequences of this for irreversible thermodynamics have been explored by D. J. Evans and H. J. M. Hanley, Phys. Lett. 80A, 175 (1980).
[7]See Ref. 4, Chap. 9 in the article by M. Reiner and G. W. Scott Blair.
[8]See the review by Y. Pomeau and Resibois, Phys. Rep.

19, 63 (1975); for the linear theory and the following papers for nonlinear results, K. Kawasaki and J. D. Gunton, Phys. Rev. A 8, 2048 (1973); T. Yamada and K. Kawasaki, Prog. Theor. Phys. 53, 111 (1975); M. H. Ernst, B. Cichocki, J. R. Dorfman, J. Sharma, and H. van Beijeren, J. Stat. Phys. 18, 237 (1978).

[9]B. J. Alder, D. M. Gass, and T. E. Wainwright, J. Chem. Phys. 53, 3813 (1970).

[10]D. J. Evans, Mol. Phys. 37, 1745 (1979).

[11]D. J. Evans, Stat. Phys. 22, 81 (1980).

[12]W. T. Ashurst and W. G. Hoover, Phys. Rev. A 11, 658 (1975).

[13]D. J. Evans, Phys. Lett. 74A, 229 (1979).

[14]D. J. Evans, Phys. Rev. A 22, 290 (1980).

[15]W. W. Wood and J. J. Erpenbeck, J. Stat. Phys. (in press).

[16]W. G. Hoover, D. J. Evans, R. B. Hickman, A. J. C. Ladd, and B. Moran, Phys. Rev. A 22, 1690 (1980).

[17]W. T. Ashurst and W. G. Hoover, Phys. Lett. 61A, 175 (1977).

[18]G. Doetsch, *Guide to the Applications of Laplace Transforms* (Van Nostrand, New York, 1961).

[19]D. A. McQuarrie, *Statistical Mechanics*, (Harper and Row, New York, 1976).

[20]P. M. Morse and H. Feshbach, *Methods of Theoretical Physics* (McGraw-Hill, New York, 1953), Part II.

[21]H. S. Green, Handb. Phys. 10, 1 (1960).

[22]D. J. Evans and H. J. M. Hanley, Physica (Utrecht), 103A, 343 (1980).

[23]L. Verlet, Phys. Rev. 159, 98 (1967).

[24]N. A. Clark and B. J. Ackerson, Phys. Rev. Lett. 44, 1005 (1980).

[25]D. J. Evans, W. G. Hoover, and A. J. C. Ladd, Phys. Rev. Lett. 45, 124 (1980).

[26]D. Levesque (unpublished data); see also Ref. 16.

[27]D. J. Evans and H. J. M. Hanley, Phys. Lett. 79A, 178 (1980).

[28]D. Beysens, M. Gbadammassi, Phys. Lett A4η, 565 (1979).

[29]D. J. Evans and H. J. M. Hanley (unpublished).

[30]Note: Orthogonality theorems show that $n > 2$ terms leave shear stress unaffected.